Workshop on sapphire detector construction

Characterization and qualification of sapphire sensors with X-rays

Sergii Vasiukov

11.01.2024

Motivation

- Ohmic or Non-Ohmic contacts
- Sapphire resistivity as a purity parameter
- Sensors response with X-ray: stability and heat-treatment

Let's try to find out

Samples under test

	Pad sensor	192 strip sensor
Sensor production	Istituto Nazionale di Fisica Nucleare (INFN)	Tomsk State University (TSU)
Sapphire production	Wuppertal (SITUS Technicals GmbH)	
Sapphire thickness	110 um	
Top layer material	Titanium + Silver (~30 nm + ~120 nm)	Chromium (~60 nm)
Back-side layer material	Titanium + Silver (~30 nm + ~120 nm)	Chromium + Nickel (~20 and 200 nm)
Sensor area	25 mm^2	400 mm^2
Capacitance	~18.9 pF	~302.5 pF

Pad sample

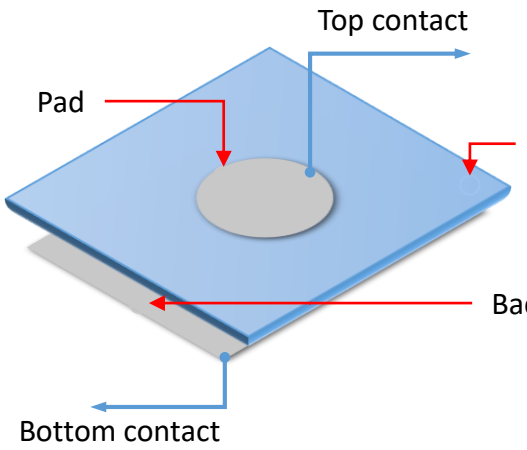

Strip sample

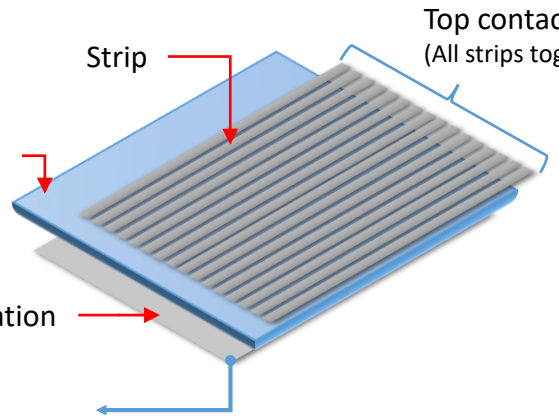

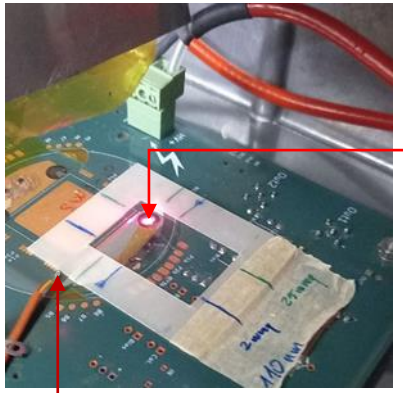

Laser spot on the sensor

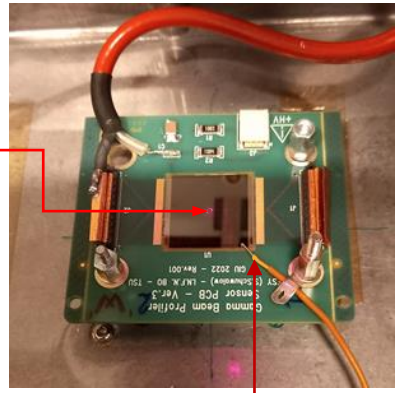

Temperature sensor on sapphire surface

Experimental setup: X-ray source

Chamber for test

X-ray tube:
W anode
Al filter

Shutter and
alignment laser

Aluminum
sample box
with heater

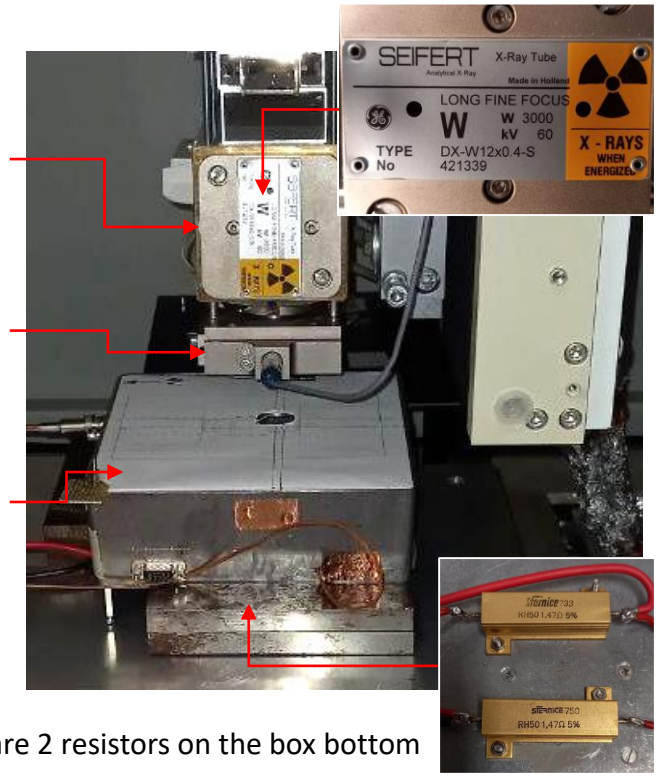

Heater: there are 2 resistors on the box bottom

X-ray spot reconstructed with Si PD
Size: ~ 33 x 33 mm at 150 mm distance

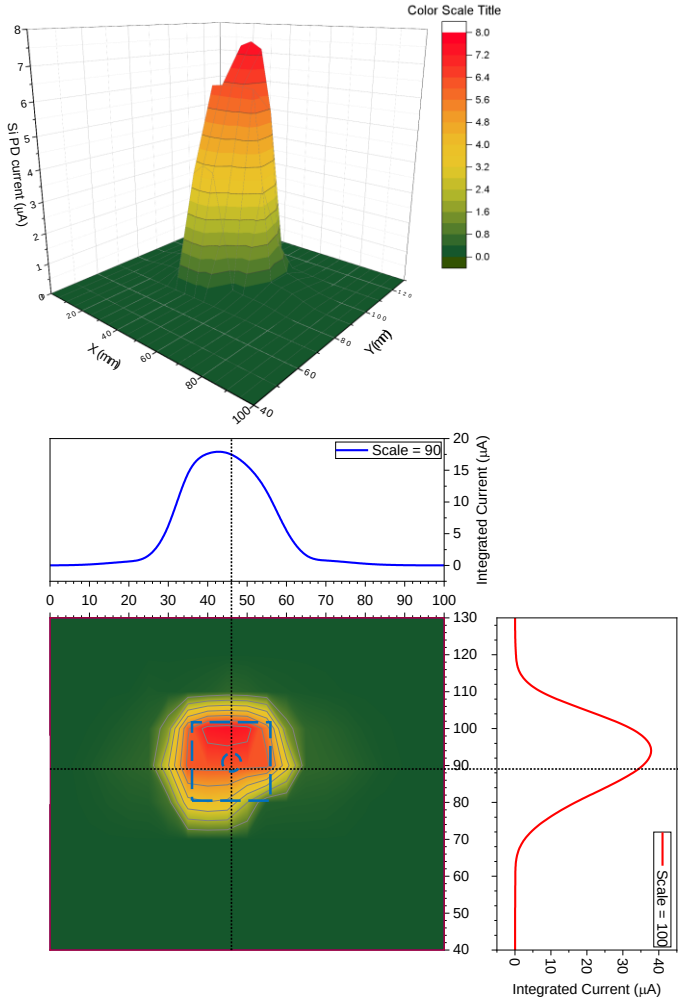

X-ray tube calibration by Si PD
I_{Si_PD} = 1 uA = 0.5888 Gy/sec

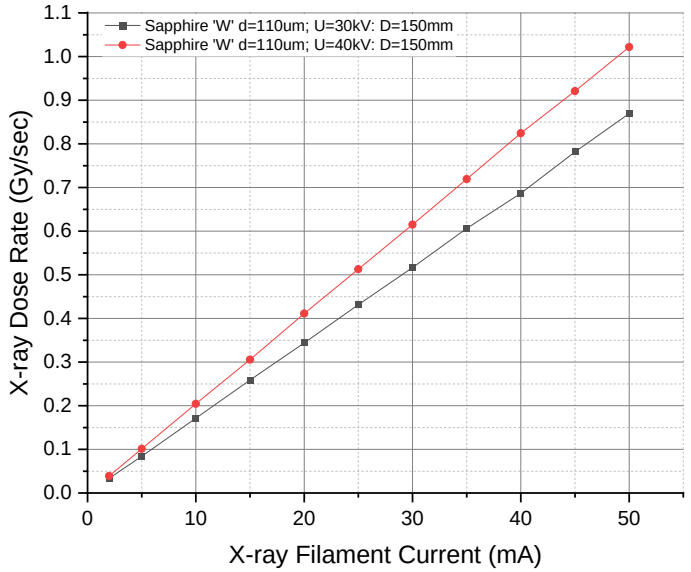

X-ray tube:
Voltage: 5 – 50 kV
Filament Current: 2 – 50 mA
Dose rate: 0.03 – 0.9 Gy/sec

Experimental setup: DC Source/Monitor and Temperature test

We can carry out the following tests:

- Current-voltage characteristic
- Current monitoring at a fixed sensor voltage bias
- Sensor current response with or without X-ray
- Temperature tests and heat treatment

The strip sensor has been heat-treated - annealing consists of gradual heating, holding at 100 °C and gradual cooling to room temperature. Details will be provided below. The set of tests was done before and after the sensor annealing.

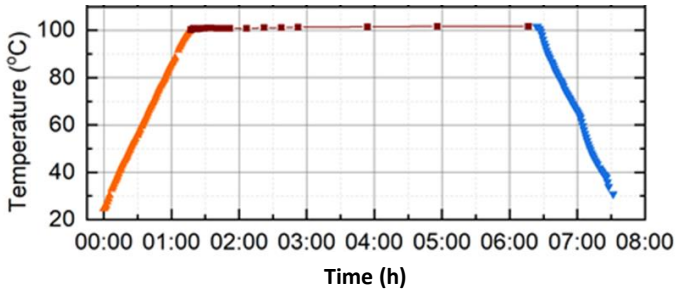

Heat/cool rate: ~1 °C/min

Temperature: 23 – 100 °C

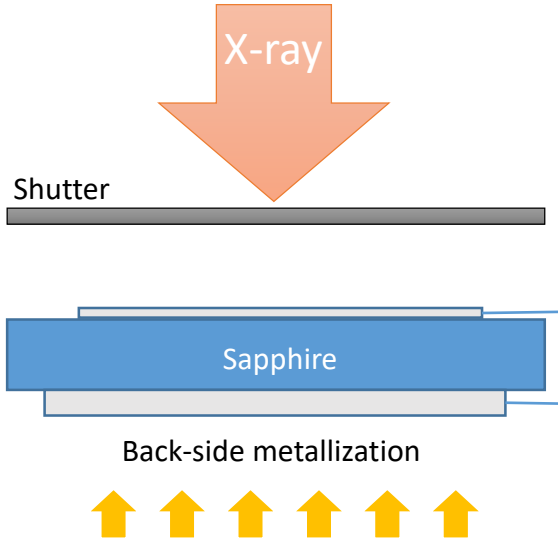

HP 4142B Modular DC Source/Monitor with HP 41420A module

Heat power supply

EA-PS 2042-20B - EA Elektro-Automatik

Current-voltage characteristics and sapphire resistivity

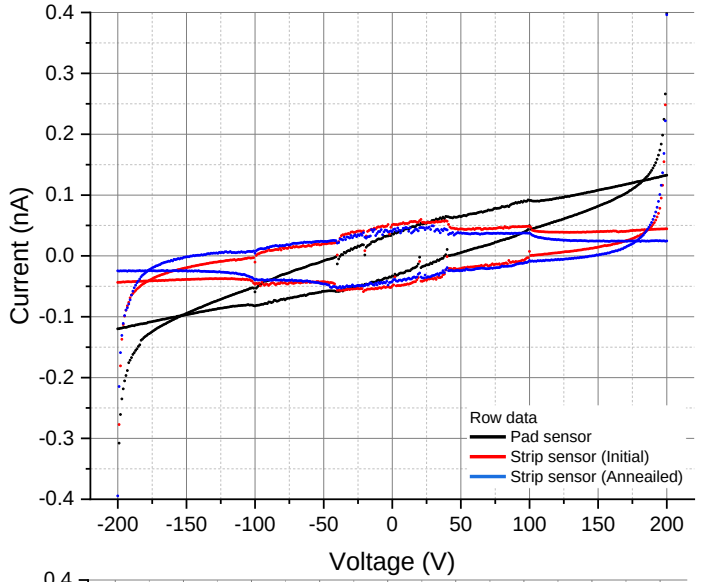

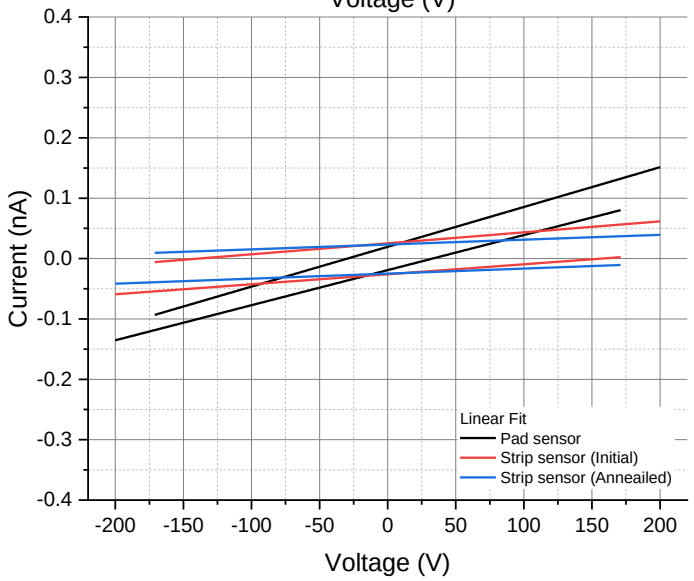

	T, °C	CVC slope [1], nA	Resistance [2], Ω	S, sq.m	d, m	Resistivity [3], Ω m
Pad sensor	27	$6.32 * 10^{-4}$	$9.07 * 10^{13}$	$2.5 * 10^{-5}$	$1.1 * 10^{-4}$	**$2.06 * 10^{13}$**
Strip sensor (Initial)	24	$1.93 * 10^{-4}$	$2.98 * 10^{14}$	$4.0 * 10^{-4}$	$1.1 * 10^{-4}$	**$1.08 * 10^{15}$**
Strip sensor (Annealed)	24	$9.48 * 10^{-5}$	$6.04 * 10^{14}$	$4.0 * 10^{-4}$	$1.1 * 10^{-4}$	**$2.20 * 10^{15}$**
Wuppertal Datasheet	25	-	-	-	-	**~ 10^{14}**

[1] Average value of the linear fit slope of CVC at voltage ramping up/down.
[2] Resistance is the cotangent of the CVC slope.
[3] Resistivity is the product of Resistance and Area of the detector (S) divided by the sapphire thickness (d).

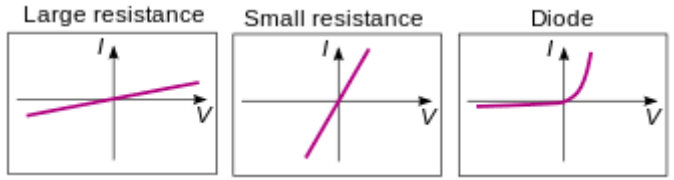

The metal layers form ohmic contacts, however, polarization distorts the linearity of the current-voltage characteristic.

A significant discrepancy in resistivity was found.

Current-voltage characteristics: X-ray

Pad sensor

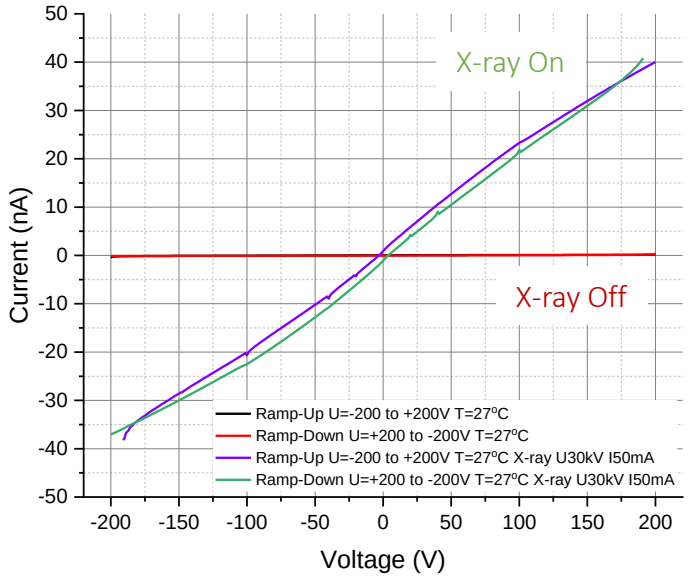

Strip sensor

Initial

1.1 nA !

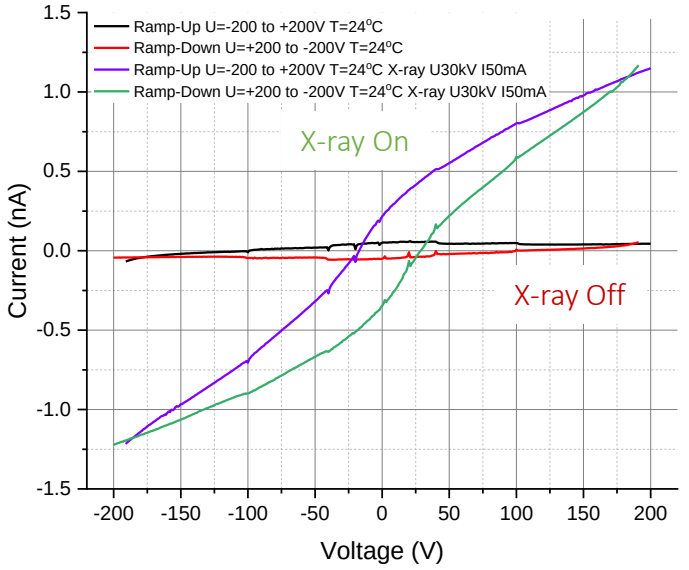

Annealed

350 nA !

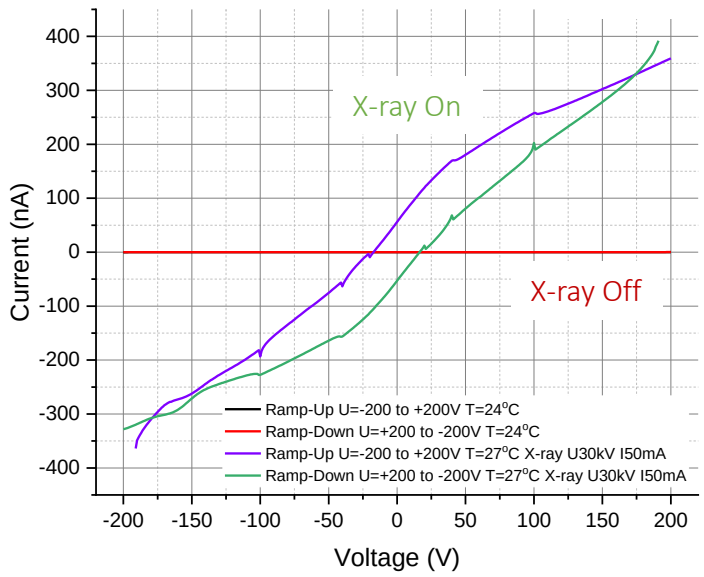

There is a smaller polarization effect on the pad sensor (less hysteresis effect) than in the case of the strip sensor.

Annealing significantly increases the strip sensor response (hundreds of times)!

Heat-treatment

What happens to the strip sensor at temperature treatment?

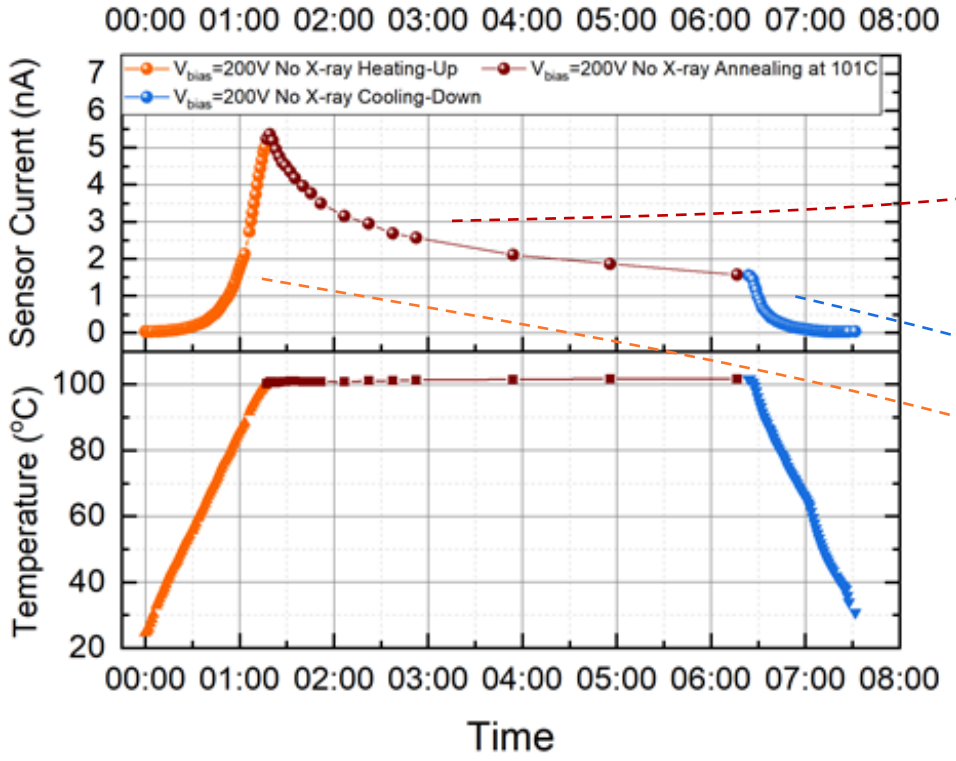

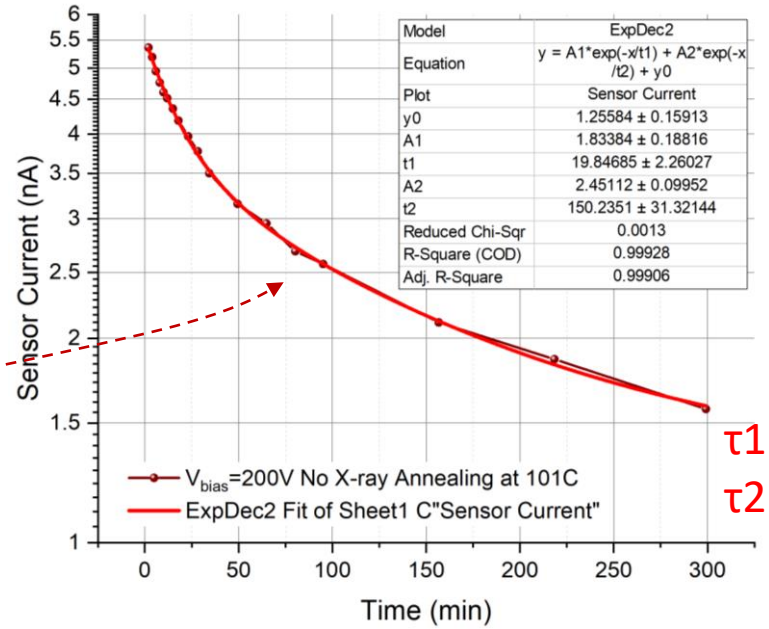

τ1 ~ 20 min
τ2 ~150 min

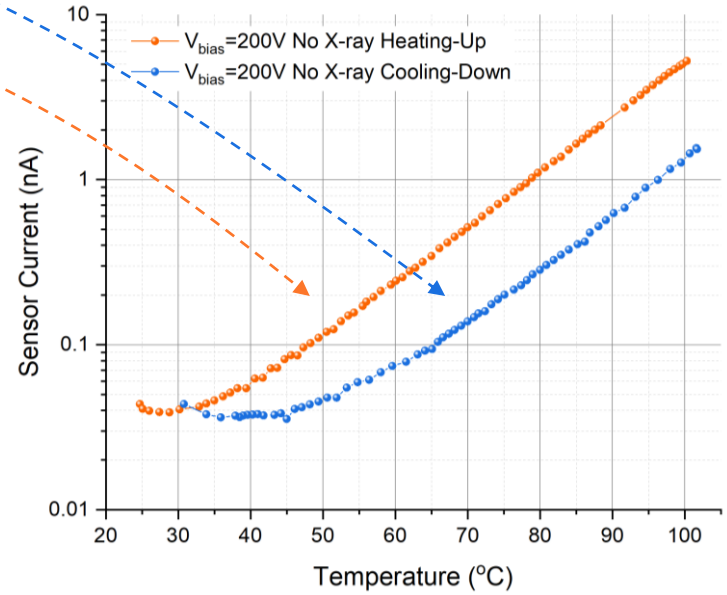

What is the main reason for this behavior?
Does relaxation of delocalized charge carriers occur at high temperatures?

Sensors response with X-ray

Pad sensor

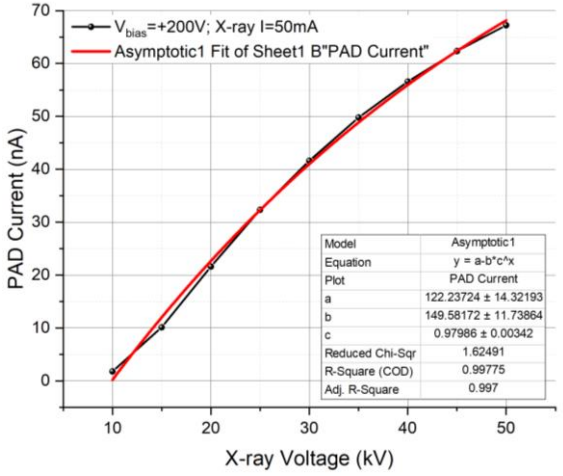

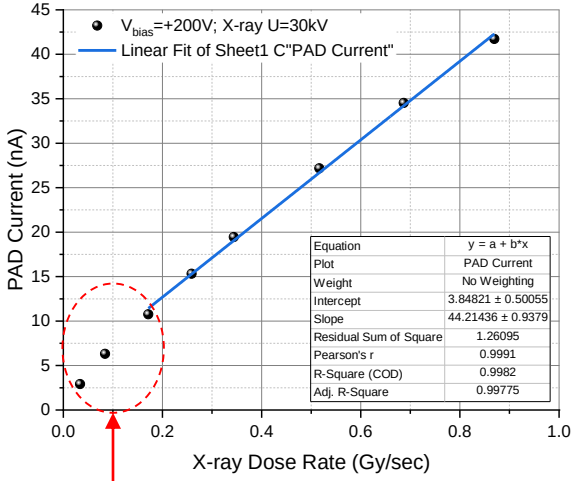

Strip sensor

Initial

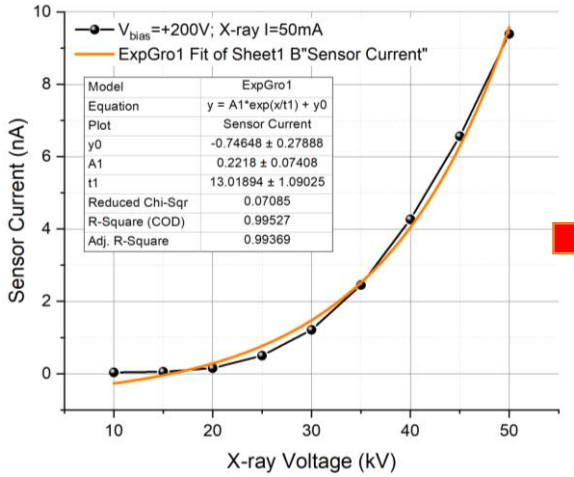

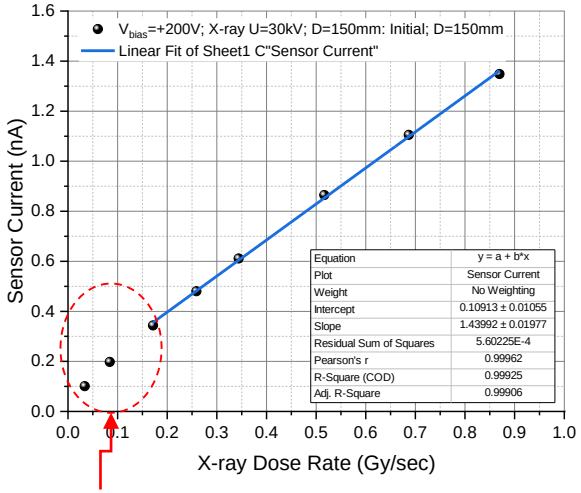

?

Annealed

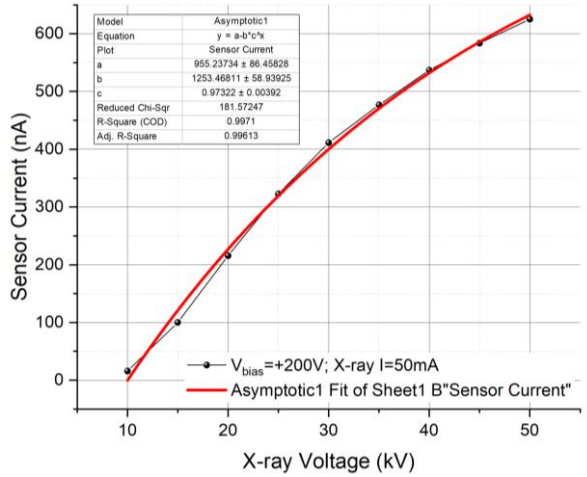

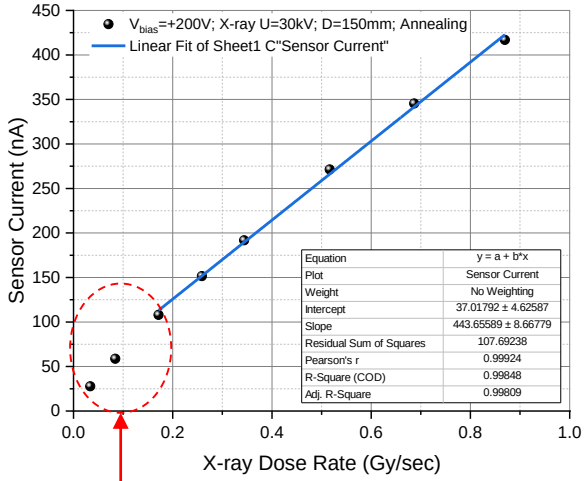

Nonlinear response, which is not observed in the case of Si PD

Questions

1. **Could the instability of the sensor response be related to the technology of metal layer deposition?**

2. **Does the instability of the sensor response mostly depend only on the quality/purity of the sapphire wafer?**

3. **The incoming control is important, but what tests are relevant?**

Thank you for attention

Temperature-stimulated current

Pad sensor

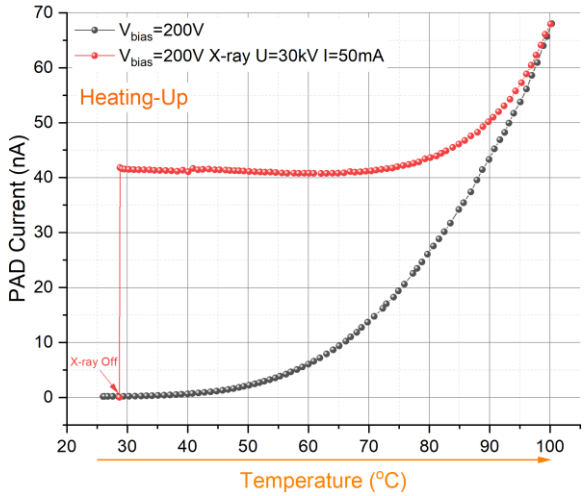

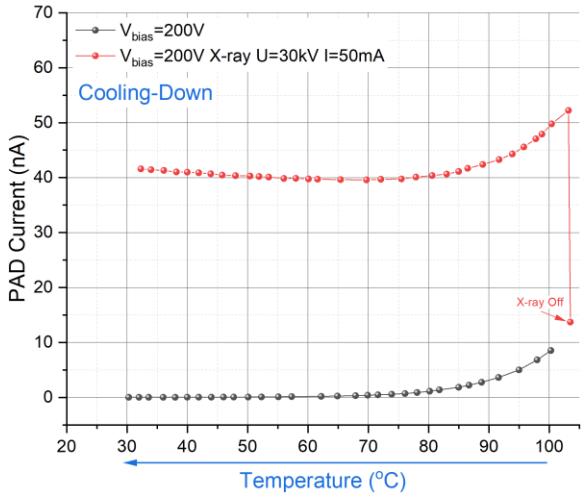

Strip sensor

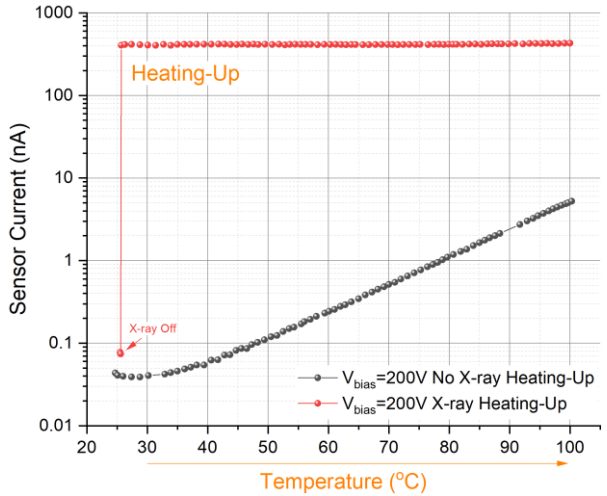

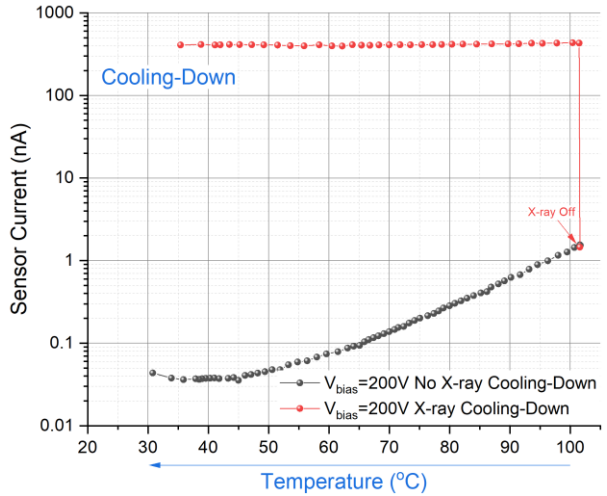

Thermo-stimulated conductivity in Al_2O_3

INFO

[D. Lapraz, S. Boutayeb, et. al., Photoinduced Thermostimulated Electrical Conductivity of an a-Al,O, Monocrystal, phys. stat. sol. (a) 136,497 (1993)]

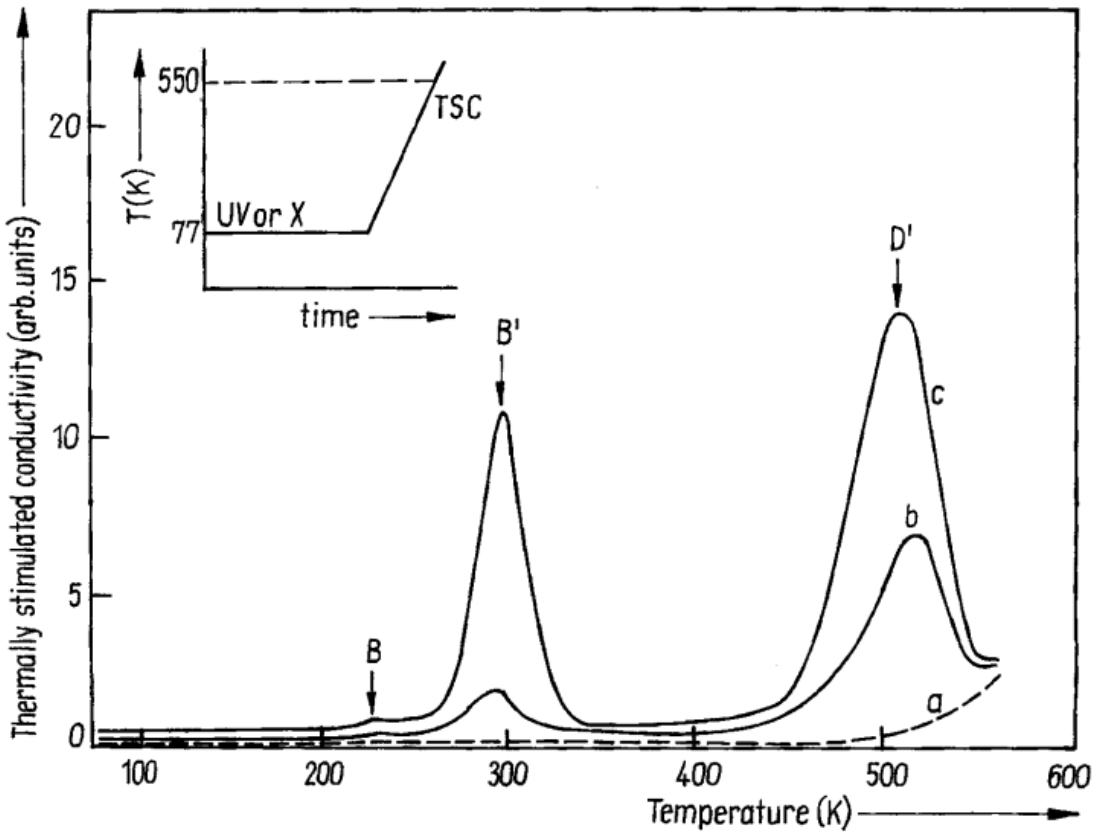

Fig. 2. Curves of TSC of α-alumina. (a) Before any irradiation, (b) after UV excitation (206 nm, 4 min) at 77 K, (c) after X-irradiation (40 kV, 86 Gy) at 77 K

'… Three TSC peaks were found in the studied crystal and correspond to the peaks called B (the weakest), B', and D'. As we can also observe these three peaks in TL, we are allowed to say first that there is a charge transfer in the course of their emission mechanism. The TL emission centres are mainly due to F' centres (320nm) for peak B, and F centres (410 nm) for peaks B' and D. Peak B' has been linked to an electron trap [4, 6, 71], peak D' either to an electron [6] or a hole [4, 5, 81], and peak B to a hole trap [4, 7, 91].'

'... the energy of X-rays, a fortiori that of UV excitation, is not sufficient to move ions of a-alumina, and therefore to increase the concentration of anion or cation vacancies [11]. So, X-irradiation simply permits the transfer of charges (electrons and holes), hence the modification of the number of charges in the metastable levels (traps).'

F and F^+ centers in Al_2O_3

INFO

[Bruce D. Evans, A review of the optical properties of anion lattice vacancies, and electrical conduction in α-Al203: their relation to radiation-induced electrical degradation, Journal of Nuclear Materials 219 (1995) 202-223]

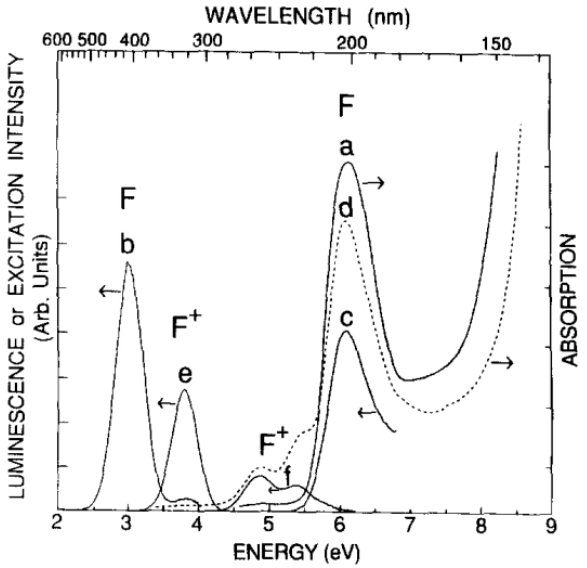

Fig. 10. Summary of optical properties of oxygen vacancy defects in single crystal α-Al_2O_3 at 300 K. Curve (a) is absorption of a growth-colored (Crystal Systems, Salem, MA) sample with peak $\alpha = 3.64\ cm^{-1}$, (b) is luminescence from the same sample with 6.0 eV excitation, (c) is an excitation spectra with the detector at 3.0 eV, curve (d) is $E \perp c$ absorption of a Czochralski-grown (Union Carbide, San Diego, CA) crystal irradiated to 1.43×10^{21} 14 MeV n/m^2 (1.8×10^{-4} dpa), peak $\alpha = 133\ cm^{-1}$, (e) is luminescence from sample in (d) with 4.8 eV excitation, and curve (f) is an excitation spectra with the detector at 3.8 eV.

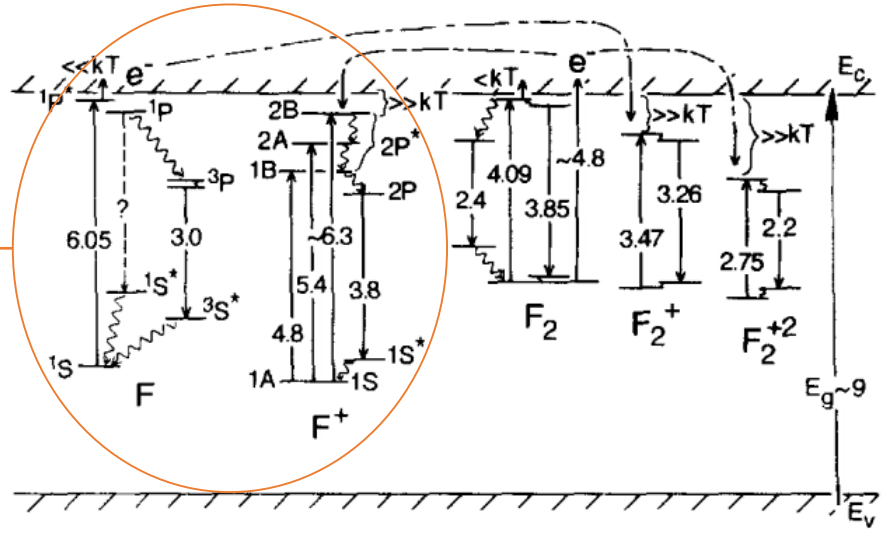

Fig. 11. Flat-band diagram of Al_2O_3 summarizing the relative energy positions of single (F-type) and paired (F_2-type) anion vacancies of different charge states.

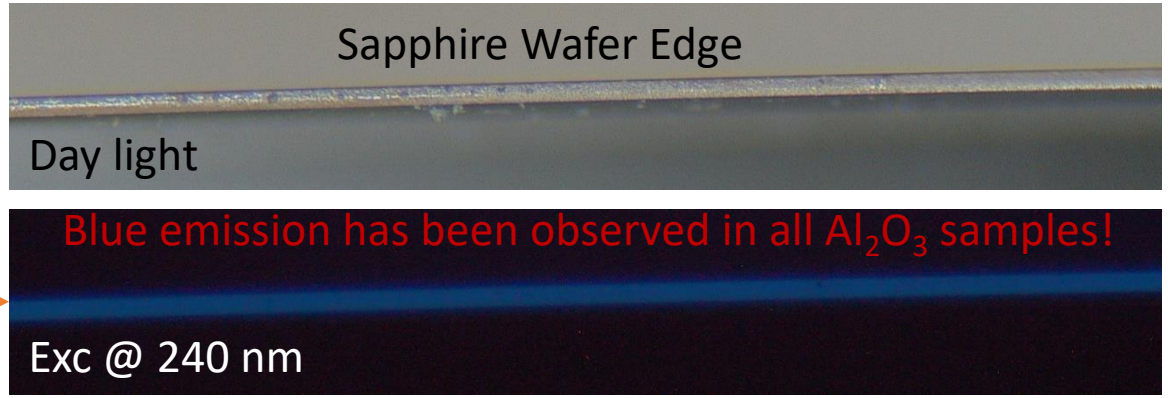

The electronic center transformation in Al_2O_3

INFO

[V.N. Kuzovkov, E.A. Kotomin, A.I. Popov, Kinetics of the electronic center annealing in Al2O3 crystals, Journal of Nuclear Materials 502 (2018) 295-300]

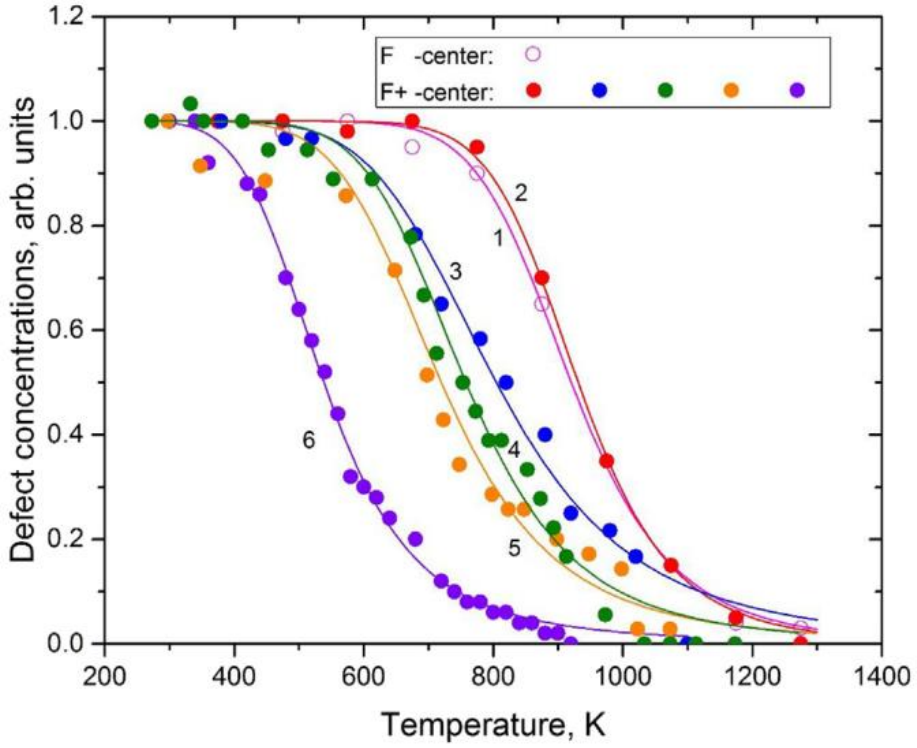

Fig. 1. The kinetics of the *F* or F^+ center annealing for different neutron fluxes (see Table 1 for details).

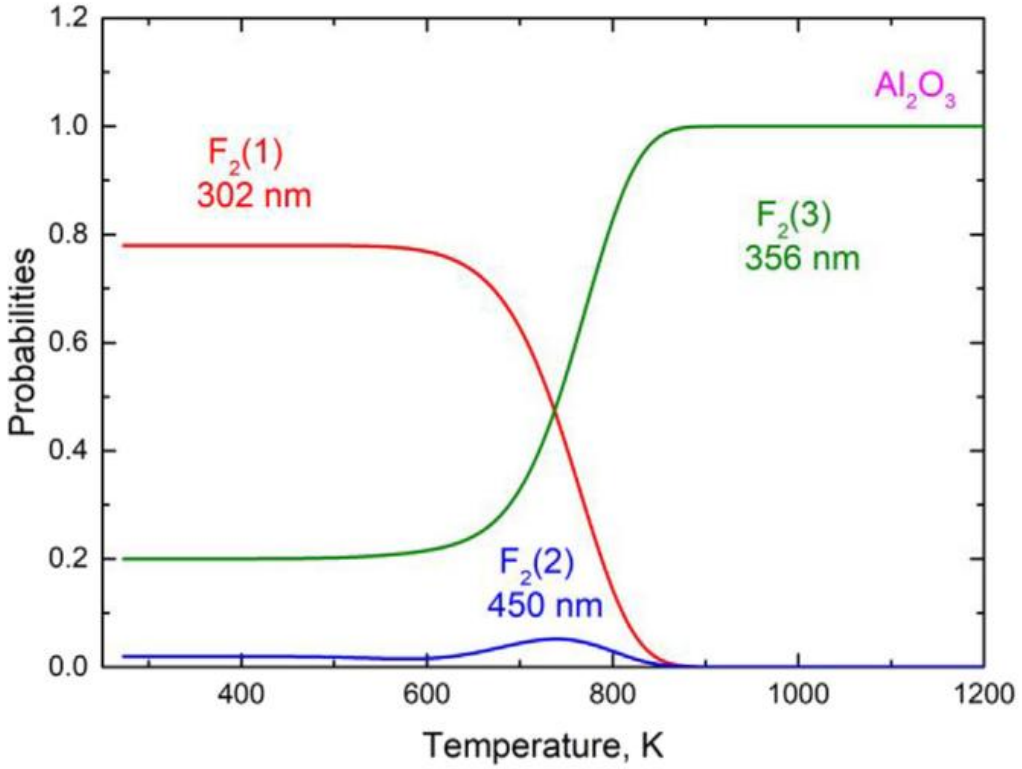

Fig. 5. Same as Fig. 4 for data in Ref. [23].

'...The main conclusions are as follows: (i) The hypothetical process $F_2(1)$ -> $F_2(3)$ does not occur, only sequential transformations $F_2(1)$ -> $F_2(2)$, $F_2(2)$ -> $F_2(3)$ take place, (ii) The rates of above mentioned reversible processes are negligibly small. Similar analysis shown that there is no mutual transformation of the F and F+ centers.'

Al_2O_3 Annealing

INFO

[Bruce D. Evans, A review of the optical properties of anion lattice vacancies, and electrical conduction in α-Al203: their relation to radiation-induced electrical degradation, Journal of Nuclear Materials 219 (1995) 202-223]

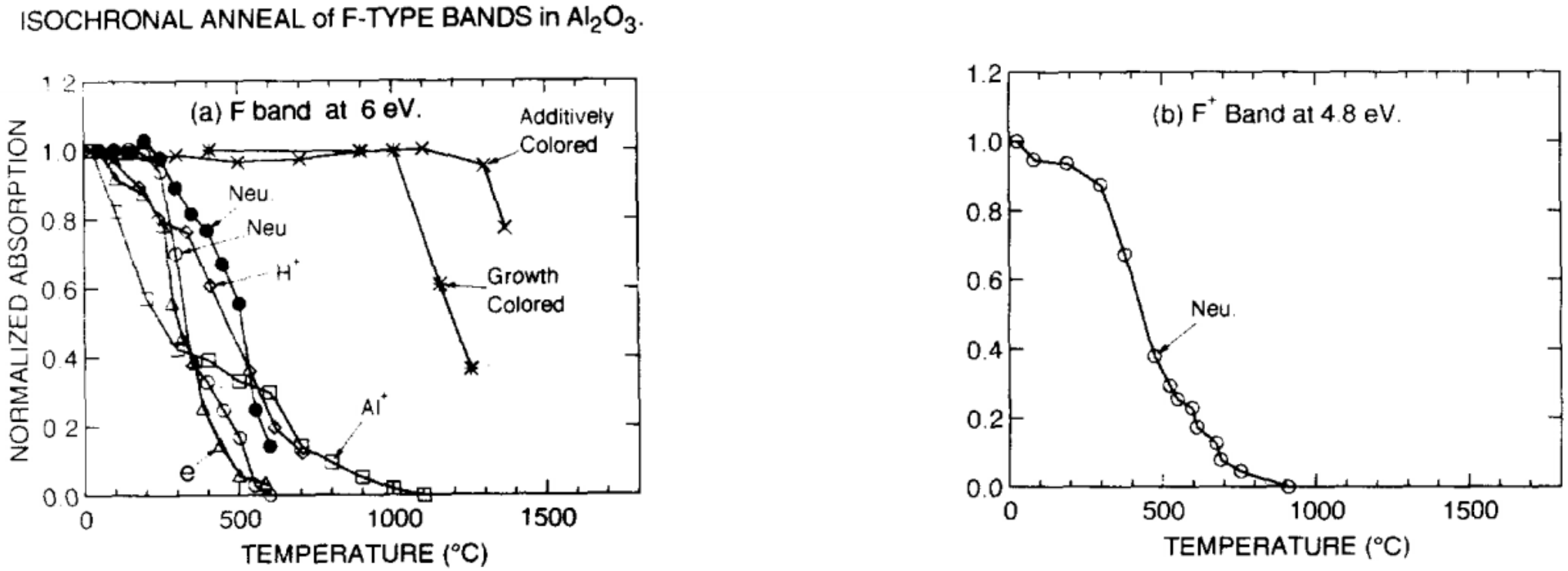

Fig. 12. Isochronal thermal anneal of (a) the 6 eV F band, and (b) the 4.8 eV F^+ band in Al_2O_3. In (a) crosses are additively colored [93]; stars, growth colored [46]; triangles, 1.5 MeV electrons at 77 K [75]; diamonds, 1.5 MeV protons [46]; circles, fission-spectrum neutrons [66]: closed without, and open with gamma exposure after each anneal step; squares, 200 keV Al^+ [69]. In (b) circles are fission-spectrum neutrons [95].

Conductivity in Al_2O_3

INFO

'… Below ~ 700°C their activation energy is about a decade lower. Low transference numbers and low self diffusion constants ruled out significant oxygen and aluminum ionic conductivity. Therefore, it was concluded that this low-temperature conductivity was of extrinsic origin. Trace levels (~ 6 ppm) of silicon found in these samples was proposed as the dominate active donor,... For example, Fe^{3+} has been reported as a typical acceptor...'

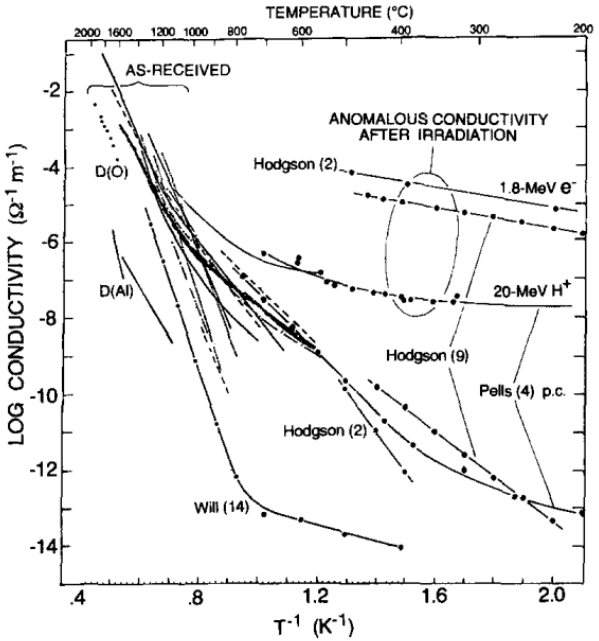

Fig. 14. Summary of electrical conductivity versus reciprocal temperature of aluminas. Data for as-received samples taken from Refs. [3,4,16,77,107,108]. Other references are shown in parentheses. D(O) and D(Al) represent conductivity due to self-diffusion of anions and cations, respectively.

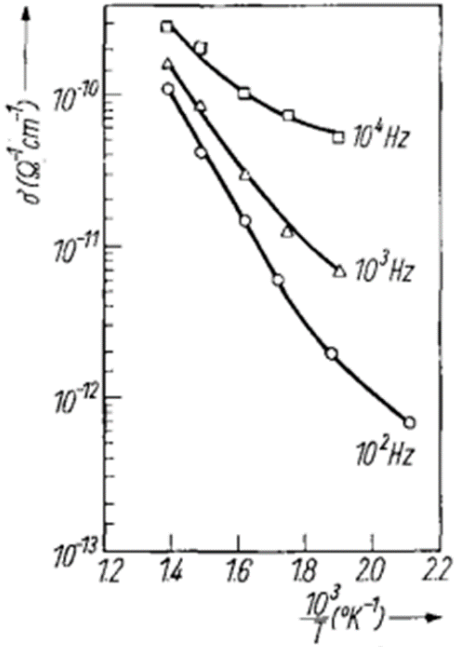

Fig. 4. Conductivity of Al_2O_3 single crystals as a function of $1/T$ at different frequencies

[Bruce D. Evans, A review of the optical properties of anion lattice vacancies, and electrical conduction in α-Al203: their relation to radiation-induced electrical degradation, Journal of Nuclear Materials 219 (1995) 202-223]

[S. Govinda and K. V. Rao, Dielectric Properties of Single Crystals of Al203 and Al2O3 Doped with Chromium or Vanadium, phys. stat. sol. (a) 27, 639 (1975)]

The transient polarization phenomena in Al_2O_3

INFO

[F. Argall and a. K. Jonscher, Dielectric properties of thin films of aluminium oxide and silicon oxide, Thin Solid Films, 2 (1968) 185-210]

'Many dielectrics show the phenomenon of anomalous absorption current upon the sudden application of a constant potential difference. Initially the current would rise quickly to well above the steady state d.c. value and would then decay over a period of time as shown in Fig. 1 for silicon monoxide. This time-dependent excess absorption current is caused by polarization in the sample. At high temperatures the steady state conduction current is attained in a matter of seconds, instead of hours as at room temperatures. At high fields, whatever the temperature, the steady state is reached almost instantly, suggesting that these polarization effects predominate only at low fields.'

'…In the Figure 2, it can be seen that at low voltages there is a distinct polarization effect which disappears at higher fields. A more detailed investigation revealed that the shallow voltage range exhibited an ohmic characteristic, and unless otherwise stated, the following results of a.c. measurements were made with a sufficiently small amplitude to fall in this ohmic region…'

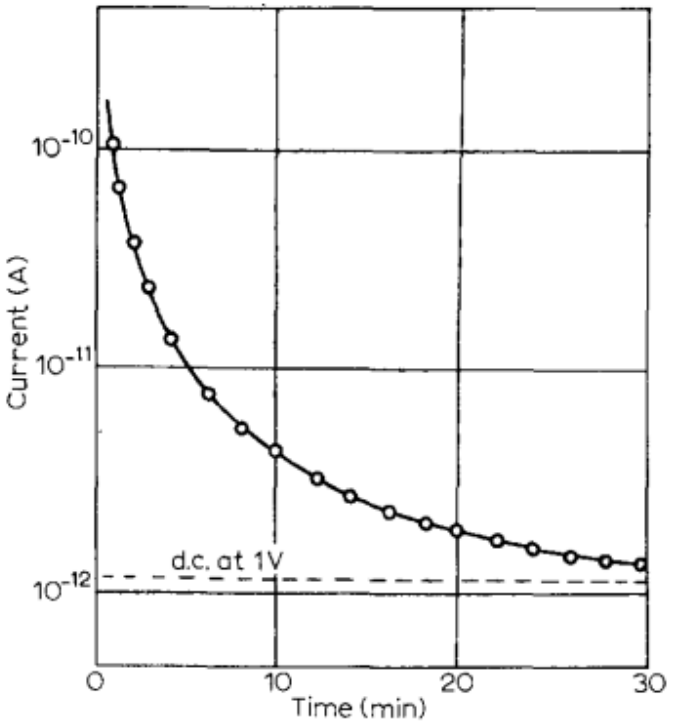

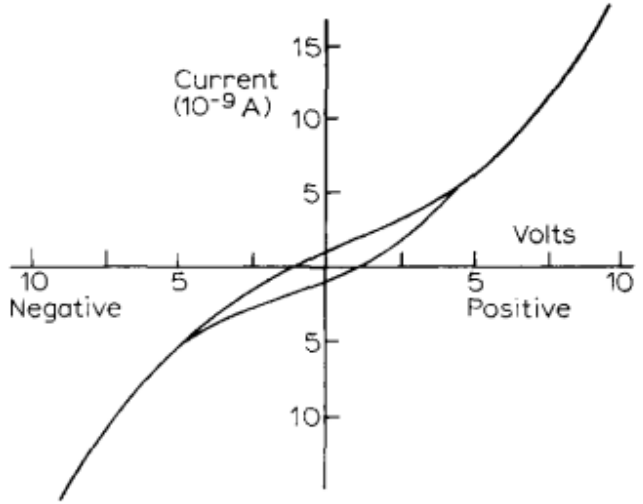

Fig. 1. Decay of absorption current with time for silicon oxide at 20 °C.

Fig. 2. Current–voltage characteristic of aluminium oxide at 22 °C using a 10^{-3} Hz triangular waveform.

The polarization phenomena in Al_2O_3

INFO

[C. Manfredotti, CVD diamond detectors for nuclear and dosimetric applications, Diamond and Related Materials Volume 14, Issues 3–7, March–July 2005, Pages 531-540]

Polarization, both in terms of decrease of counting rate and signal, is an effect related either to poor charge collection properties, or to a lack of full depletion of the detector, or, better, to both of them. Lack of full depletion is due to a not sufficiently low net impurities concentration, or even to a drop of the electrical field at one or both of the contacts because of technological deficiencies. This is not related only to CVD or natural diamond, but also to CdTe, which is much more technologically developed (see for instance Fig. 3 of Ref. [7]) and it was extensively investigated by ion beam induced current or charge (IBIC), which makes use of scanning proton microbeams either on electrode surfaces of detectors (frontal IBIC) or on suitably prepared (cleaved and possibly passivated) cross-sections of detectors themselves (lateral IBIC) in order to obtain maps of charge collection efficiency (cce).

In fact, neither alpha particle spectra [1] nor frontal IBIC spectra [8] were correctly recorded because of extremely fast polarization effects (few seconds) which quickly pushed the relevant peak in the multichannel spectrum to the low energy side. This is not a particular case of low efficiency CVD diamond samples, but it could occur also in higher efficiency ones: only some high purity natural diamond samples exhibited high collection efficiencies at high counting rates.

Frontal IBIC measurements (cce maps and profiles) are possible in thin samples, which do not suffer from polarization effects, because they are fully depleted and contact effects are less important. An example is given by btipQ diamond detectors, which have been obtained by deposition of CVD diamond on tungsten tips [9]–realized in the same way as AFM cantilever tips–up to a thickness of 10–20 Am (Fig. 1): cce profile and maps–as taken perpendicularly to tip axis–were quite easy to carry out and even quite uniform, particularly at low bias voltages.

In effect, if polarization is due to poor contacts, it may affect not only pc, but also sc CVD diamond sample, as it was the case of bdetector gradeQ CdTe, particularly for thick samples. The presence of bpoorQ contacts is indicated by a decay of cce at contacts in cce maps and profiles obtained by lateral IBIC. This seems not to be the case of natural diamond, where the lateral IBIC map (Fig. 2a) is quite uniform up to the electrodes (which are vertical on both sides of the figure) and the relevant cce profile (Fig. 2b) shows a sharp decay at both sides. The slow increase of cce as a function of bdecadeQ (i.e., one tenth of the total dose delivered to the sample by protons during the scan over the investigated surface) is due to a priming effect, which will be described in the next paragraph. Polarization gives rise to some strange effect, such as polarity inversion of charge pulses, when bias voltage is switched off: the internal electrical field due to polarization shows itself as a peak of cce for instance at one electrode (see for instance Fig. 5 of Ref. [7]). Lateral IBIC maps of CVD samples are generally not uniform both because of columnar structure and because of short ccd with respect to sample thickness, which gives rise to low values of cce in the central part (see Fig. 3), which is distant from both electrodes and from which charge collection is more difficult for both carriers, because drift time becomes longer than trapping time. The build-up of space charge in the central region lowers the local electrical field and increases the electrical field in the two regions aside. The irregular profile at the right electrode (growth side) is due to surface morphology, since the sample is not polished. In case of priming (see the upper part of the map), cce is much more uniformly distributed, as probably also the electrical field, and space charge has almost disappeared.

The polarization phenomena in Al_2O_3

INFO

[R. C. Hughes, Generation, transport, all trapping of excess charge carriers in Czochralski-grown sapphire, PHYSICAL REVIEW B, Vol. 19, No 10, 1979]

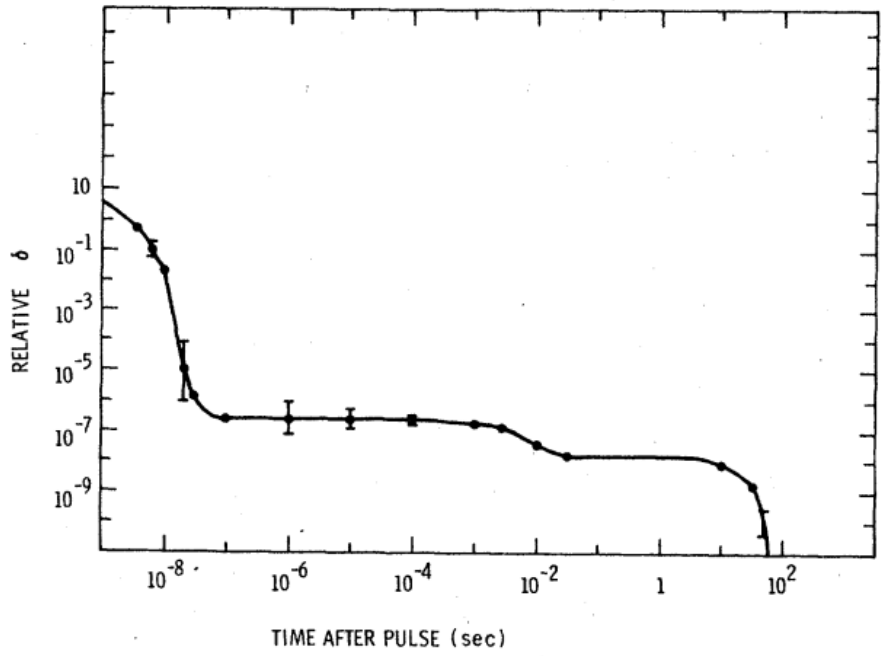

FIG. 1. Log–log plot of the relative conductivity vs time for a typical sapphire sample at 300 °K. The applied field and the number of excess carriers are kept low enough so that all conductivity decays depicted are due to first-order trapping kinetics. The excitation pulse is 3×10^{-9} sec wide. The error bars reflect the experimental error in taking the derivative of charge collection data in the given time ranges.

'High-energy X-rays produce a nearly uniform distribution of electrons and holes in the bulk of the sapphire crystal. The excess conductivity of these carriers can be measured by their displacement current in an applied field. Figure 1 gives the conductivity over many orders of magnitude under conditions which guarantee that no significant number of carriers is lost by bulk recombination or sweeping out to the electrodes, and that there are no space charge induced distortions in the photocurrent profiles. The decay in the conductivity is then caused solely by first-order trapping kinetics. There are four distinct regions in the conductivity curve: (i) a prompt, high-mobility component which decays exponentially with a time constant of a few nanoseconds over several orders of magnitude, (ii) and (iii) there are two plateaus in the conductivity with the higher one decaying into the lower with a time constant of about $2*10^{-3}$ sec, and (iv) the conductivity decays, again exponentially, to levels below our detectability with a time constant of a few seconds, at room temperature.

The data are suggestive of trap modulation of the carrier mobility in which there are at least three traps. Two of the traps have release rates greater than 1 sec^{-1}, which create the two plateaus. The release rate of the third is too low to be detected at room temperature, but may be observed in higher-temperature thermally stimulated current (TSC) experiments and/or thermally stimulated luminescence (TSL) experiments. Table I gives the values for the long-term lifetime (τ3) in the samples that were investigated…'

The conductivity in Al_2O_3

INFO

[B.P. Aduev, E.D. Aluker, and V.N. Shvaiko, Radiation induced conductivity in α Al2O3 crystals, Phys. Solid State 39 (11), 1997]

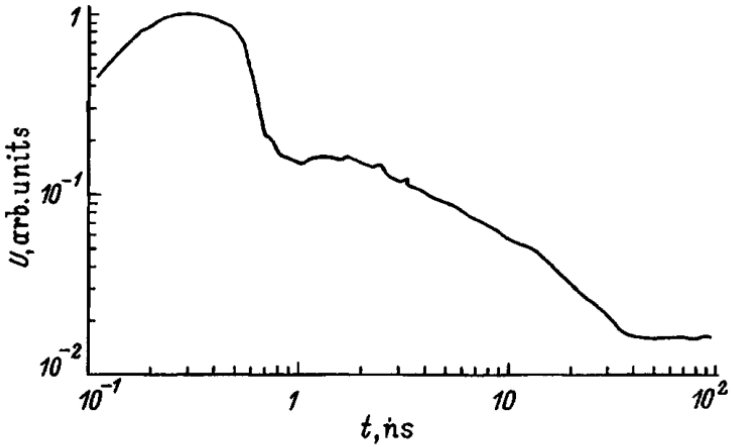

FIG. 1. Relaxation of the conduction current in α Al_2O_3.

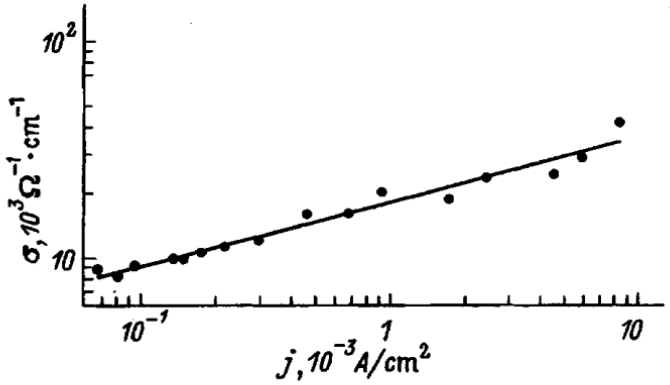

FIG. 2. The conductivity σ as a function of beam current density j in α Al_2O_3.

'…The relaxation of the conduction current over a wide time interval is shown in Fig. 1. The current reaches a maximum at 300 ps, which corresponds to the transient response of the measurement circuit. This implies that a component of the conduction current which follows the exciting pulse without delay is not observed, as, for example, in crystalline NaCl and KCl. Then a subnanosecond decay takes place which does not fit a simple pattern and this is followed, to within the limits of sensitivity of the apparatus, by at least two further relaxation components of the conduction current in the nanosecond range. The current-voltage characteristics measured from the amplitudes of the conduction current are linear in fields up to at least $5*10^4$ V/cm. The conductivity was calculated from the current-voltage characteristics. The experiment was repeated over a wide range of excitation current densities *j* and the result is shown in Fig. 2. *σ(j)* has a power law dependence, $\sigma \infty j^{\alpha}$, with α=0.3. This is a very important result. If the subnanosecond component of the conduction current, making up > 0.9 of the current amplitude, were caused by electrons from the conduction band or holes from the valence band prior to recombination or capture by defects, then we should have $\sigma \infty j$. Our result indicates that the lifetime of the band carriers prior to capture is of order $\tau \leq 10^{-10}$ s. Thus, the observed components of the relaxing conduction current, including the fastest, are caused by thermal release of carriers from traps and their subsequent redistribution. Here at least three types of traps are observed.'

Sapphire: Resistivity vs Temperature

INFO

[P. Pavlasek et. al. Effects of Quartz Glass Insulation on Platinum Gold Thermocouples, Measurement science review, 19, (2019), No. 5, 209-212]

$2*10^{11}$ Ω m

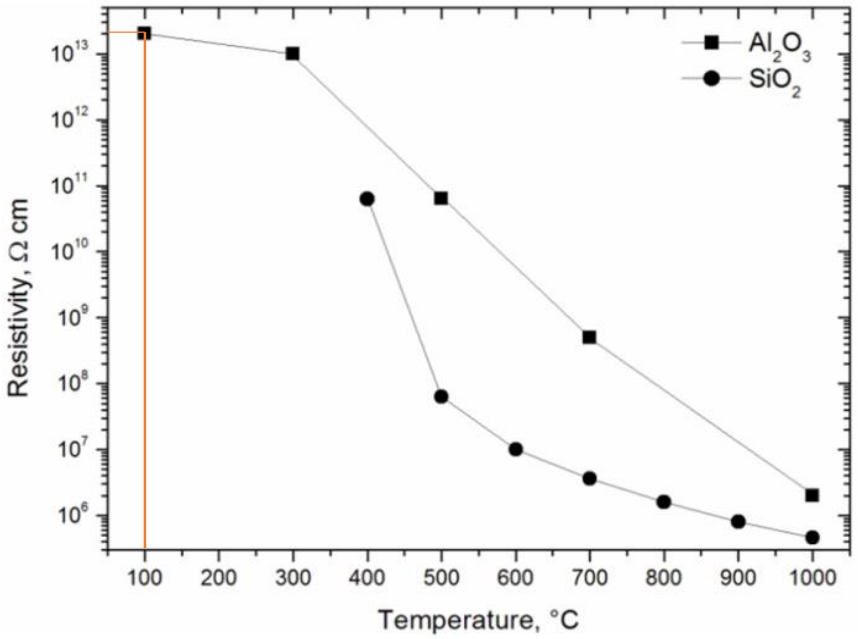

Fig.2. Resistivity of quartz glass (SiO_2) and aluminium oxide (Al_2O_3) at elevated temperatures [16].